PLANT SCIENCE

Evolution of carnivorous traps from planar leaves through simple shifts in gene expression

Christopher D. Whitewoods[1]*, Beatriz Gonçalves[1]*, Jie Cheng[1,2,3]*, Minlong Cui[4], Richard Kennaway[1], Karen Lee[1], Claire Bushell[1], Man Yu[1], Chunlan Piao[4], Enrico Coen[1]†

Leaves vary from planar sheets and needle-like structures to elaborate cup-shaped traps. Here, we show that in the carnivorous plant *Utricularia gibba*, the upper leaf (adaxial) domain is restricted to a small region of the primordium that gives rise to the trap's inner layer. This restriction is necessary for trap formation, because ectopic adaxial activity at early stages gives radialized leaves and no traps. We present a model that accounts for the formation of both planar and nonplanar leaves through adaxial-abaxial domains of gene activity establishing a polarity field that orients growth. In combination with an orthogonal proximodistal polarity field, this system can generate diverse leaf forms and account for the multiple evolutionary origins of cup-shaped leaves through simple shifts in gene expression.

Leaves come in many shapes and sizes. Most consist of planar sheets of cells that harvest light for photosynthesis. Formation of these leaves depends on adaxial and abaxial domains of gene activity in leaf primordia (*1*, *2*). However, the mechanism by which these domains generate sheet-like development is unclear. It is unknown whether growth is oriented by the adaxial-abaxial (ad-ab) boundary throughout the leaf or solely at the epidermis. It is also unclear how orientations of growth and cell division are specified and whether growth orients the plane of division or the plane of division orients growth. Finally, it is unclear how the system for planar leaf development has been modified to generate nonplanar leaves, such as filiform (needle-like) leaves and cup-shaped leaves of carnivorous plants, which have evolved multiple times independently (*3*).

Computational models for formation of flat or cup-shaped leaves have been proposed based on cell divisions being induced by the epidermal ad-ab boundary, with the plane of division orienting growth (*4*, *5*). However, these models are not easily reconciled with observations that cell divisions occur throughout the leaf lamina, not solely at the margin (*6*–*8*). Here, we suggest an alternative mechanism based on the analysis of ad-ab genes in trap and filiform leaf development of the humped bladderwort, *Utricularia gibba* (Lentibulariaceae), an aquatic carnivorous plant (Fig. 1, A to F).

Each *U. gibba* leaf consists of several filiform leaflets (Fig. 1, B, E and F) and may bear a trap (Fig. 1, D and F). At early developmental stages, organ primordia are dome-shaped (Fig. 1G). On the basis of morphology alone, it is unclear at this stage whether these primordia will become leaflets or traps. At later stages, leaflet primordia form tapering cylinders that grow to be slightly wider than thick and curve longitudinally toward the apex (Fig. 1, H to J). By contrast, trap primordia are curved in both longitudinal and transverse sections and consist of three cell layers (Fig. 1K). The inner layer is positioned adaxially (facing the spiral apex, the right-hand side of the images in Fig. 1). As development progresses, the trap grows to a near-spherical shape with a closed mouth (Fig. 1, L to M, white arrowheads), and a two-cell-thick trap door grows out near the dorsal lip (Fig. 1, N and O, orange arrowheads). Over a 20-fold increase in trap length (about 400-fold increase in area), lamina thickness only doubles (Fig. 1, K to O, and fig. S1), resulting in a curved sheet.

To define the ad-ab domains in *U. gibba* (*9*, *10*), we identified homologs (named with Ug prefix) of the adaxially expressed *PHV* and *PHB* genes and abaxially expressed *FIL* and *KAN* genes (*1*, *11*). Before trap and leaflet primordia morphologies clearly diverged, *UgPHV1* was expressed on the adaxial side (black arrowhead in Fig. 2A) and was more restricted in some primordia (yellow arrowhead in Fig. 2A). In leaflet primordia at later stages, *UgPHV1* and *UgFIL1* were expressed on the adaxial and abaxial sides, respectively (Fig. 2, B to E, and fig. S3, A to J). In trap primordia, *UgPHV1* was expressed in the innermost cell layer, extending into the inner side of the trap door (Fig. 2, F to I, and fig. S3, K to P). *UgFIL1* and *UgKAN1* were expressed in the outer layers (Fig. 2, J to Q, and fig. S3, Q to V), although only *UgKAN1* was expressed in the outer ventral region (yellow arrowheads in Fig. 2, N to Q). Thus, the adaxial and abaxial domains of a planar leaf broadly correspond to the inner and outer regions of the trap, respectively. Similar findings were reported for the *Sarracenia purpurea* trap, although *KAN* expression was not detected (*5*).

To determine whether the observed expression patterns have functional importance, we induced ectopic expression of microRNA-resistant *UgPHV1* under the control of the 35S promoter, using a Cre-Lox system (*HS-UgPHV1* plants, see methods for details). After extended heat shock, green fluorescent protein fluorescence and in situ hybridization confirmed ectopic induction throughout the tissue (fig. S4).

To determine how ectopic *UgPHV1* affected development, tissues were imaged daily after induction (Fig. 3, A to D). At 7 days post-induction (Fig. 3D), the main axis could be divided into three regions. (i) An upper region, encompassing the apex and leaves (Fig. 3D, red). The normal spiral organization of the apex had been replaced by an open linear structure (Fig. 3, H to M), containing no trap primordia and only radially symmetrical leaflets (fig. S5). The leaves below the apex bore no traps or bore small malformed traps (Fig. 3D and fig. S6, C to E). Tracing this upper region back through the sequence of daily images showed it derived from primordia located within the spiral apex at the time of induction (Fig. 3C and fig. S6B). (ii) A middle region (Fig. 3D, blue) derived from leaves bearing small traps (80 to 200 μm long) at the time of induction (Fig. 3C). This region had normal leaves bearing traps up to 300 μm long (Fig. 3D, white arrowheads, and fig. S6B), with thick walls and malformed trap doors (fig. S6, F to H). (iii) A lower region (Fig. 3D, black) derived from leaves bearing traps that were longer than 200 μm at the time of induction (Fig. 3C). This region contained normal leaves and traps (Fig. 3D, black arrowheads, and fig. S6B).

Thus, ectopic expression of *UgPHV1* in early primordia leads to loss of trap development (Fig. 3, E and F) and generation of radialized organs, similar to the effect of ectopic *PHV* and *PHB* expression in *Arabidopsis* (*11*–*13*). Ectopic *UgPHV1* expression in later trap primordia, but before traps are 200 μm long, leads to aberrant trap development and growth arrest (Fig. 3G and fig. S6). Ectopic *UgPHV1* expression after this stage has no effect, although this may be due to inefficiency of induction in older traps (fig. S4). These results indicate that restricted *UgPHV1* expression is necessary for initiation and maintenance of trap development.

To explore how domains of ad-ab identity may control leaf morphogenesis, we modeled

[1]Department of Cell and Developmental Biology, John Innes Centre, Norwich Research Park, Colney Lane, Norwich NR4 7UH, UK. [2]State Key Laboratory of Systematic and Evolutionary Botany, CAS Center for Excellence in Molecular Plant Sciences, Institute of Botany, Chinese Academy of Sciences, Beijing 100093, China. [3]College of Life Sciences, University of Chinese Academy of Sciences, Beijing 100049, China. [4]College of Agriculture and Food Science, Zhejiang Agriculture and Forestry University, Linan 311300, Zhejiang, China.
*These authors contributed equally to this work.
†Corresponding author. Email: enrico.coen@jic.ac.uk

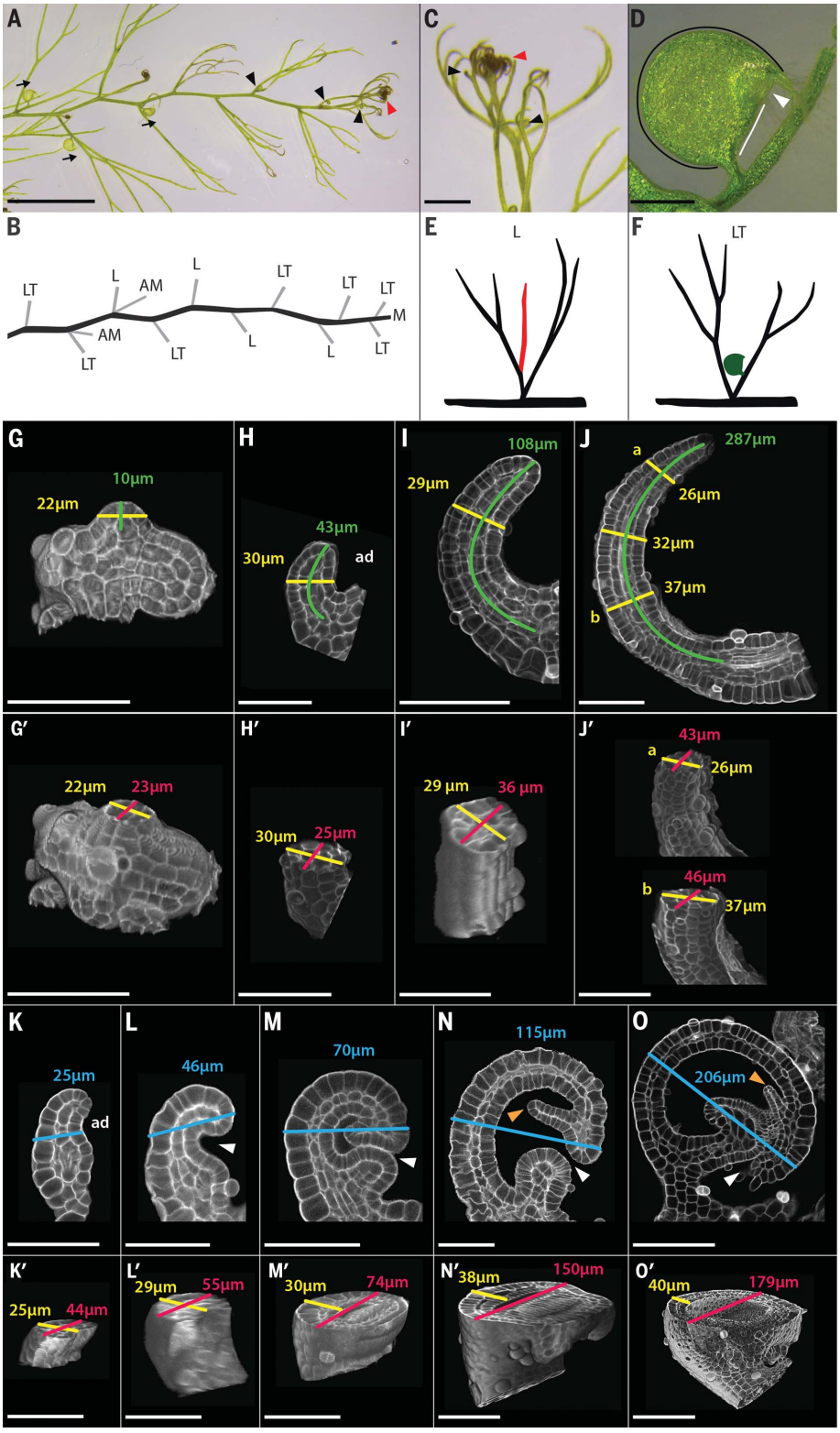

Fig. 1. *U. gibba* morphology. (**A**) Stolon with circinnate apex (red arrowhead) bearing leaves and traps (black arrowheads) oriented adaxially (black arrows). (**B**) Schematic of (A) showing stolons (black) and leaves (gray). L, leaflet-bearing leaf; LT, trap-bearing leaf; AM, axillary meristem; M, apical meristem. (**C**) Magnification of apex shown in (A). (**D**) Trap showing dorsal (black line) and ventral (white line) sides and mouth (white arrowhead). (**E**) Diagram of a leaflet-bearing leaf in (B), with one leaflet in red. (**F**) Diagram of a trap-bearing leaf in (B), with a trap in green. (**G** and **G**) Confocal micrographs of early primordium, in longitudinal (G) and transverse section viewed obliquely (G′). (**H** to **J**) Confocal micrographs of a developmental series of leaflets in longitudinal [(H) to (J)] and transverse sections viewed obliquely [(H′) to (J′)]. (**K** to **O**) Confocal micrographs of a developmental series of traps in longitudinal [(K) to (O)] and transverse sections viewed obliquely [(K′) to (O′)]. In (G) to (O′), green lines mark primordium and leaf length; yellow lines mark primordium, leaf, and trap thickness; red lines mark primordium, leaf, and trap width; and blue lines mark trap length. Measurements are given in the same colors as the lines (see fig. S1 for additional data). In (N) and (O), orange arrowheads mark the trap door, and white arrowheads mark the trap mouth. In (D), (H) to (O′) organs are shown with the adaxial side to the right, marked "ad" in (H) and (K). Scale bars are 5 mm in (A), 1 mm in (C), 500 μm in (D), 50 μm in [(G), (G′), (H), (H′), (I), (I′), (J′), and (K) to (N′)], and 100 μm in [(J), (O), and (O′)]. The image in (N) was previously published in (*26*).

primordia as mechanically connected viscoelastic volumes of material, with growth oriented by a polarity field (*14*). We began with a hemispherical ground state, representing a radialized leaf primordium without a history of ad-ab activity, with polarity pointing proximodistally (red arrows in Fig. 4A). For simplicity, the field was implemented by taking the gradient of a morphogen diffusing from the base toward the tip. In reality, such fields most likely reflect cellular polarity rather than a continuous field (*15*, *16*). Specifying a higher growth rate parallel to, rather than perpendicular to, the polarity generated a tapering cylinder, corresponding to the phenotype

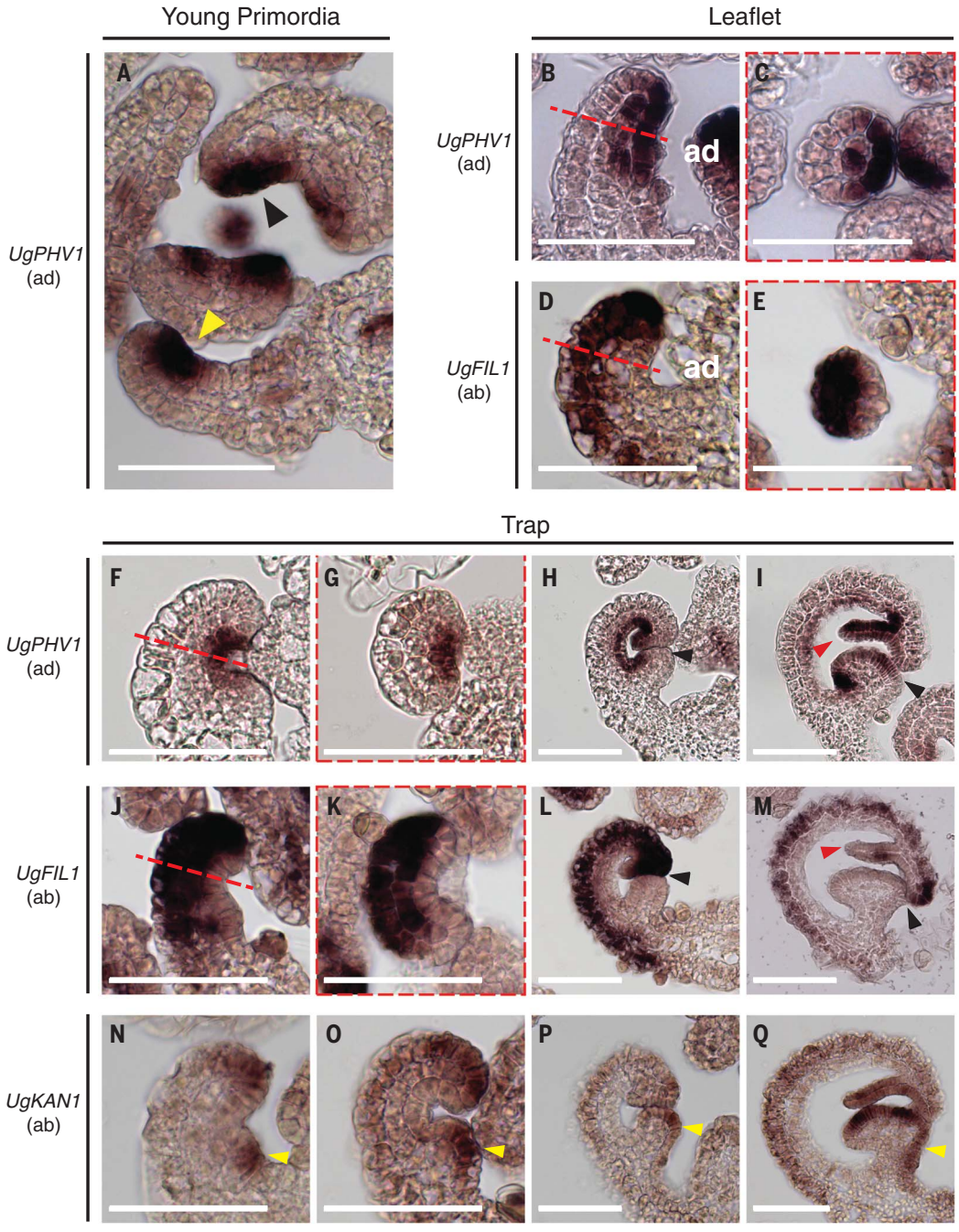

Fig. 2. *UgPHV1* and *UgFIL1* expression patterns in *U. gibba* leaflet and trap development. (**A**) *UgPHV1* expression in young primordia. Black and yellow arrowheads mark primordia that show extended and restricted domains of the adaxial marker, respectively. (**B** to **E**) *UgPHV1* [(B) and (C)] and *UgFIL1* [(D) and (E)] in leaflet primordia. (**F** to **I**) *UgPHV1* during trap development, in longitudinal [(F), (H), and (I)] and cross (G) sections. (**J** to **M**) *UgFIL1* expression during trap development in longitudinal [(J), (L), and (M)] and cross (K) sections. (**N** to **Q**) *UgKAN1* expression during trap development in longitudinal sections. The dashed red lines in (B), (D), (F), and (J) indicate the angle of cross sections shown in (C), (E), (G), and (K), respectively. Trap mouth (black arrowheads), trap door (red arrowheads), and ventral regions (yellow arrowheads) are indicated. In all panels, the adaxial side is shown to the right, marked "ad" in (B) and (D). Scale bars are 50 μm. See an expanded version of this figure in fig. S3.

of radialized mutants (Fig. 4, A to C, and movie S1).

To model formation of a planar leaf, we invoked a second polarity field, orthogonal to the first, termed the orthoplanar polarity field (black arrows in Fig. 4D). This field was implemented by taking the gradient of a morphogen diffusing from the outer surface of the primordium toward the junction between the adaxial and abaxial domains throughout the midplane. Evidence for a midplane domain playing a role in lamina formation comes from analysis of the *WOX-PRS* module (*17*–*20*). Three growth rates could then be specified: parallel to proximodistal polarity (K_{pd}), parallel to the orthoplanar polarity (K_{op}), and perpendicular to both (K_{per}) (*14*) (Fig. 4E).

Setting K_{op} to be much lower than K_{pd} and K_{per} generated a flattened sheet, corresponding to a planar leaf (Fig. 4, F and G, and movie S2). Similar results were obtained using elliptical or elongated initial primordium shapes, illustrating the robustness of the model (fig. S7). Low K_{per} as well as K_{op} generated a tapering elliptic cylinder, corresponding to a leaflet of *U. gibba* (Fig. 4, H and I, and movie S3). Thus, the formation of a planar leaf can be accounted for by having relatively low K_{op}, and the formation of a filiform leaf by both low K_{op} and low K_{per}.

To determine the effect of a more confined adaxial domain, as observed in some *U. gibba* primordia (yellow arrowhead in Fig. 2A), we restricted the domain to a small region on one side of the primordium while keeping the same values of K_{per}, K_{op}, and K_{pd} as in the planar leaf model (Fig. 4, J and L). Running this model generated a cup-shaped sheet

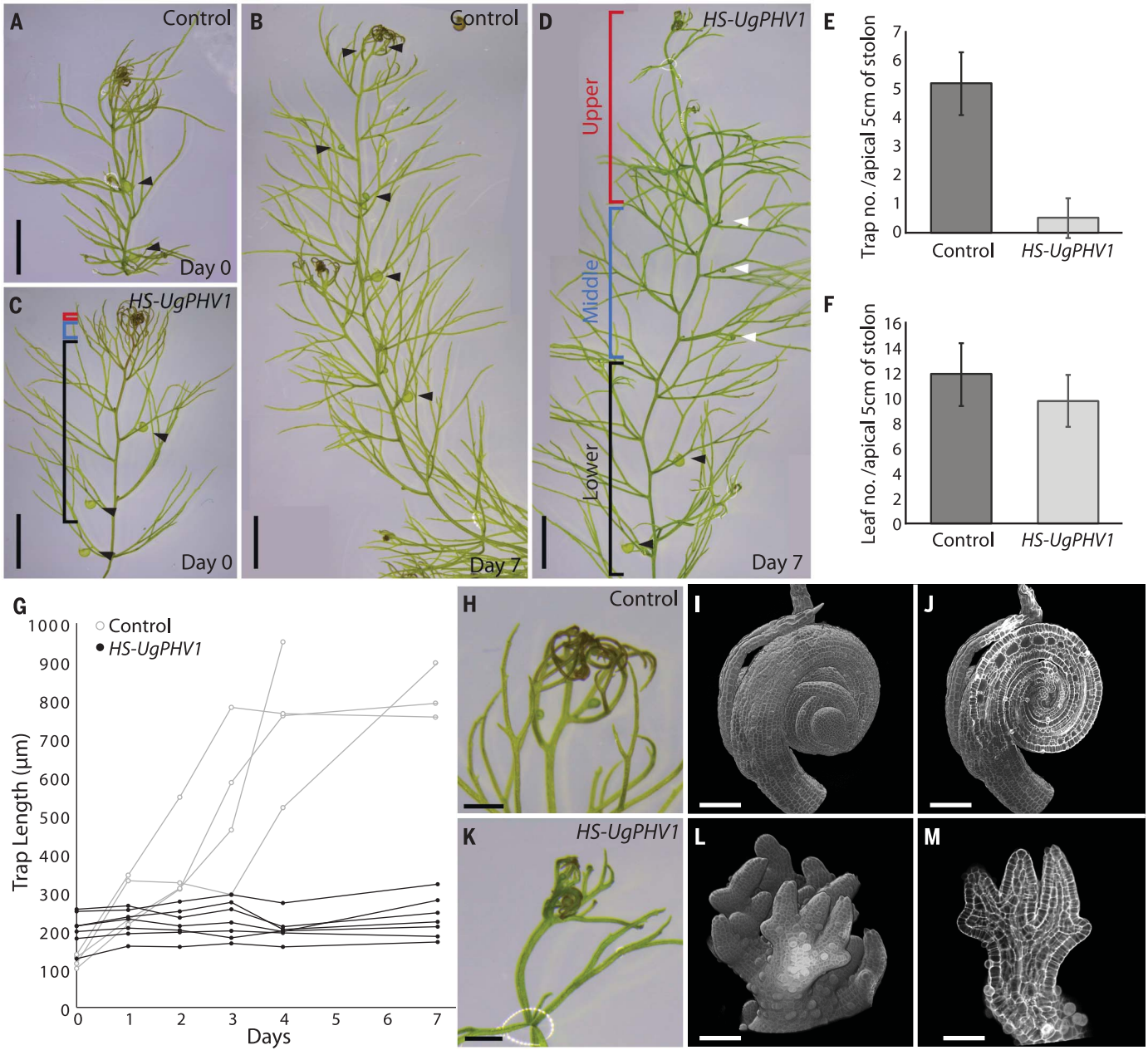

Fig. 3. Induction of *UgPHV1* prevents trap formation. (**A** to **F**) Uninduced plants (control) produce traps (black arrowheads) at regular intervals [(A) and (B)], whereas induction of *UgPHV1* prevented new trap formation [(C), (D), and (E)] and trap growth (white arrowheads) but not leaf formation (F). (**G**) Upon induction, traps smaller than 200 μm did not grow. (**H** to **J**) Apex of control plants showing circinate structure in confocal images [(I) and (J)]. (**K** to **M**) Apex of induced plants showing open structure and straight leaves in confocal images [(L) and (M)]. Scale bars are 5 mm in (A) to (D), 1 mm in (H) and (K), 100 μm in (I) and (J), and 50 μm in (L) and (M).

with the adaxial domain on the inner surface (Fig. 4, K and L, and movie S4). This result suggests that those primordia showing restricted *PHV1* expression at early stages (Fig. 2A) are fated to form traps. The model also predicts that expressing the adaxial domain throughout the primordium eliminates the orthoplanar polarity field, generating a tapering cylinder (Fig. 4B), consistent with the results of ectopic *PHV1* expression (Fig. 3 and fig. S6).

In contrast to *U. gibba*, the adaxial domain in trap primordia of *S. purpurea* extends to the base of the primordium as a narrow ventral strip, which grows out to form a ridge (*5*). Incorporation of such a strip within the above model led to the formation of a cup with a ridge, similar to the form observed in *S. purpurea* (Fig. 4, M to P, and movie S5). In *S. purpurea*, cell divisions were observed to be preferentially periclinal (new cell walls parallel to the outer surface of the primordium) in the ridge-forming region but not in the more distal cup-forming region (*5*). Fukushima *et al.* incorporated these observations into a two-dimensional (2D) model of a transverse section of the primordium, with small outgrowths prespecified at the ad-ab boundary. Assuming divisions are induced near the epidermal ad-ab boundary and that the planes of division determine the orientation of growth, this model could generate the observed 2D shapes (*5*).

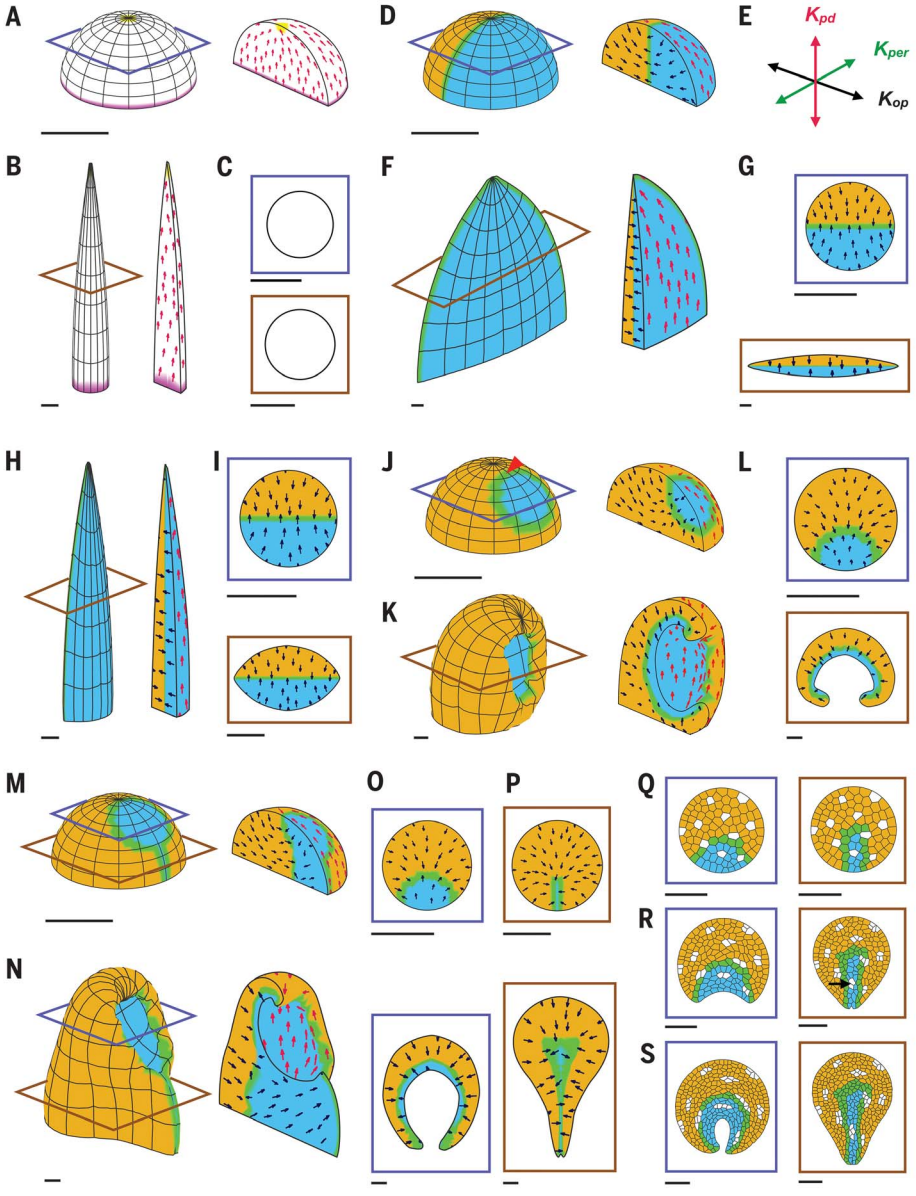

Fig. 4. Modeling of leaf and trap development. Oblique, cutaway, and section views. (**A** to **C**) Generation of tapering cylinder. Initial [(A) and top of (C)] and final [(B) and bottom of (C)] states are shown. Proximodistal polarity (red arrows) runs from organizers at the base (magenta) to the tip (yellow). (**D** to **G**) Generation of flat sheet. Initial [(D) and top of (G)] and final [(F) and bottom of (G)] states are shown. Adaxial (blue), abaxial (brown), and midplane (green) domains are shown. Orthoplanar polarity (black arrows) runs from surface to midplane. Proximodistal and orthoplanar polarity are shown only on outer and cutaway surfaces, respectively. Three growth rates (K_{pd}, K_{op}, and K_{per}) are specified by two polarity fields (E). (**H** and **I**) Generation of an elliptic cylinder. Final state [(H) and bottom of (I)] and initial state [top of (I)]. (**J** to **L**) Generation of a cup. Red arrowhead indicates shifted position of sink for proximodistal polarity. Initial [(J) and top of (L)] and final [(K) and bottom of (L)] states. (**M** to **P**) Generation of cup with ridge. Initial [(M) and top of (O) and (P)] and final [(N) and bottom of (O) and (P)] states. (**Q** to **S**) 2D models showing cell division patterns corresponding to section levels shown in (M) and (N). Initial (Q), intermediate (R), and final (S) states. Periclinal division walls in ridge are indicated by the arrow in (R). Levels of transverse sections are indicated by color-coded rectangles. Scale bars represent the same length in all panels and are in arbitrary units.

To determine whether our model would give similar division patterns, we modeled transverse sections of the primordium containing virtual cells (Fig. 4Q), with specified growth oriented relative to an orthoplanar polarity field. The plane of cell division was set by taking the shortest path through the cell center (*6*, *21*). Some cells were marked in white to allow clones to be visualized. Running this model recapitulated the observed patterns of division (Fig. 4, R and S, and movies S6 and S7), with divisions in the ridge-forming region being preferentially periclinal (black arrow in Fig. 4R). Thus, our model accounts for both trap morphogenesis and observed planes of division in *S. purpurea*.

Our findings provide a simple mechanistic explanation for the generation of planar, filiform, and cup-shaped leaves, through shifts in expression domains or their effects on growth. Unlike previous models, growth is oriented by a polarity field, anchored by ad-ab domains acting throughout the leaf (not just at the epidermal boundary), consistent with observed division patterns. The planes of division are a result (emergent property) of, rather than the cause of, oriented growth. Moreover, our model does not depend on the primordium already having outgrowths in the regions that form the lamina, showing that it can break morphological symmetry rather than simply elaborating it.

Additional structures, such as petioles, can be generated by introducing further domains into the model (figs. S8 to S10 and movies S8 to S10). Diverse shapes and patterns of dissection in the outline of planar leaves may also be generated through modulation of growth oriented by a proximodistal polarity field (*22*–*25*). Thus, a system in which regional identities modify growth rates oriented by two orthogonal polarity fields provides developmental flexibility and can account for how cup-shaped forms evolved multiple times independently from species with planar leaves.

REFERENCES AND NOTES

1. J. R. McConnell, M. K. Barton, *Development* **125**, 2935–2942 (1998).
2. R. Waites, A. Hudson, *Development* **121**, 2143–2154 (1995).
3. A. M. Ellison, N. J. Gotelli, *J. Exp. Bot.* **60**, 19–42 (2009).
4. Y. Hayakawa, M. Tachikawa, A. Mochizuki, *J. Theor. Biol.* **404**, 206–214 (2016).
5. K. Fukushima *et al.*, *Nat. Commun.* **6**, 6450 (2015).

6. S. Fox *et al.*, *PLOS Biol.* **16**, e2005952 (2018).
7. K. J. I. Lee *et al.*, *PLOS Biol.* **17**, e3000427 (2019).
8. R. S. Poethig, I. M. Sussex, *Planta* **165**, 170–184 (1985).
9. E. Ibarra-Laclette *et al.*, *Nature* **498**, 94–98 (2013).
10. T. Lan *et al.*, *Proc. Natl. Acad. Sci. U.S.A.* **114**, E4435–E4441 (2017).
11. J. R. McConnell *et al.*, *Nature* **411**, 709–713 (2001).
12. J. F. Emery *et al.*, *Curr. Biol.* **13**, 1768–1774 (2003).
13. K. R. Siegfried *et al.*, *Development* **126**, 4117–4128 (1999).
14. R. Kennaway, E. Coen, *Open Biol.* **9**, 190057 (2019).
15. K. Abley *et al.*, *Development* **140**, 2061–2074 (2013).
16. C. Mansfield *et al.*, *Curr. Biol.* **28**, 2638–2646.e4 (2018).
17. H. Lin *et al.*, *Proc. Natl. Acad. Sci. U.S.A.* **110**, 366–371 (2013).
18. M. Nakata *et al.*, *Plant Cell* **24**, 519–535 (2012).
19. M. Vandenbussche *et al.*, *Plant Cell* **21**, 2269–2283 (2009).
20. M. J. Scanlon, R. G. Schneeberger, M. Freeling, *Development* **122**, 1683–1691 (1996).
21. L. Errera, *C. R. Acad. Sci.* **103**, 822–824 (1886).
22. T. Blein *et al.*, *Science* **322**, 1835–1839 (2008).
23. A. Hay, M. Tsiantis, *Nat. Genet.* **38**, 942–947 (2006).
24. E. E. Kuchen *et al.*, *Science* **335**, 1092–1096 (2012).
25. A. Richardson, A. B. Rebocho, E. Coen, *Plant Cell* **28**, 2079–2096 (2016).
26. C. D. Whitewoods, E. Coen, *Curr. Biol.* **27**, R910–R918 (2017).

ACKNOWLEDGMENTS

We would like to thank B. and P. Steward at The Fly Trap Plants and T. Bailey from the Carnivorous Plant Society for plants, seeds, and advice. **Funding:** This work was supported by a European Research Council grant (323028-CarnoMorph) and Biotechnology and Biological Sciences Research Council grants (BBS/E/J/000PR9787, BB/M023117/1, and BB/L008920/1) awarded to E.C. C.B. was funded by grant 1243441 from the Biotechnology and Biological Sciences Research Council. B.G. was supported by a Long-Term Fellowship from the Federation of European Biochemical Societies. J.C. was supported by the University of Chinese Academy of Sciences Joint Ph.D. Training Program and a National Natural Science Foundation of China grant (91631308). **Author contributions:** C.D.W. and B.G. performed biological experiments and data analysis and contributed to conceptualization; J.C. performed computational modeling and data analysis and contributed to conceptualization; M.C. and C.P. performed plant transformation; R.K. performed software development and computational modeling; K.L. developed *U. gibba* resources; C.B. performed RNA sequencing and data analysis; M.Y. performed biological experiments and data analysis; and E.C. supervised the research, performed funding acquisition, and contributed to conceptualization. **Competing interests:** The authors declare no competing interests. **Data and materials availability:** All data are available in the main text or the supplementary materials. Code is available at the following websites: https://github.com/JIC-Enrico-Coen/GFtbox_CarnivorousTraps_2019 and http://cmpdartsvr3.cmp.uea.ac.uk/wiki/BanghamLab/index.php/Software.

SUPPLEMENTARY MATERIALS

science.sciencemag.org/content/367/6473/91/suppl/DC1
Materials and Methods
Figs. S1 to S10
Tables S1 to S6
References (*27*–*35*)
Movies S1 to S10
Data S1

View/request a protocol for this paper from *Bio-protocol*.

28 June 2019; accepted 12 November 2019
Published online 21 November 2019
10.1126/science.aay5433